

Article

Development of Auto-Seeding System Using Image Processing Technology in the Sapphire Crystal Growth Process via the Kyropoulos Method

Churl Min Kim ¹, Sung Ryul Kim ^{1,*} and Jung Hwan Ahn ²

¹ Precision Manufacturing & Control R&D Group, Korea Institute of Industrial Technology, 1,30, Gwahaksandan 1-ro 60 beon-gil, Gangseo-gu, Busan 46742, Korea; chmikim@kitech.re.kr

² School of Mechanical Engineering, Pusan National University, 2, Busan daehak-ro 63 beon-gil, Geumjeong-gu, Busan 46241, Korea; jhwahn@pusan.ac.kr

* Correspondence: sungkim@kitech.re.kr; Tel.: +82-051-974-9259

Academic Editor: Giorgio Biasiol

Received: 2 February 2017; Accepted: 5 April 2017; Published: 7 April 2017

Abstract: The Kyropoulos (Ky) and Czochralski (Cz) methods of crystal growth are used for large-diameter single crystals. The seeding process in these methods must induce initial crystallization by initiating contact between the seed crystals and the surface of the melted material. In the Ky and Cz methods, the seeding process lays the foundation for ingot growth during the entire growth process. When any defect occurs in this process, it is likely to spread to the entire ingot. In this paper, a vision system was constructed for auto seeding and for observing the surface of the melt in the Ky method. An algorithm was developed to detect the time when the internal convection of the melt is stabilized by observing the shape of the spoke pattern on the melt material surface. Then, the vision system and algorithm were applied to the growth furnace, and the possibility of process automation was examined for sapphire growth. To confirm that the convection of the melt was stabilized, the position of the island (i.e., the center of a spoke pattern) was detected using the vision system and image processing. When the observed coordinates for the center of the island were compared with the coordinates detected from the image processing algorithm, there was an average error of 1.87 mm (based on an image with 1024 × 768 pixels).

Keywords: sapphire; single crystal growth; Kyropoulos method; auto-seeding; image processing; spoke pattern

1. Introduction

Single-crystal sapphire is a material that has high hardness, excellent chemical stability, and optical transparency in a wide range of wavelengths. Due to these advantages, it is widely used in various industries including engineering, military supply, aviation, optics, and healthcare. At present, large quantities of sapphire ingots are being produced due to the prevalence of light-emitting diode back light units (LED BLUs), which use sapphire substrates, and the demand for this material is increasing rapidly [1]. Accordingly, many studies are being conducted on the production of large-diameter single crystals because they provide greater benefits than small-diameter single crystals in terms of productivity and market price.

For the growth of large-diameter single-crystal sapphire, the Kyropoulos (Ky) and Czochralski (Cz) methods are predominately used. The Cz method is a wide spread single crystal growth technique in which alumina is melted in a crucible and the seed is pulled up; the seed is simultaneously rotated after it contacts the surface of the molten metal [2]. The Ky method is mainly used for the single crystal growth of large-diameter sapphire. Though its basic growth furnace is similar to that of the

Cz method, the seed is not rotated after it contacts the molten alumina, but the heater temperature is slowly lowered so that the single crystal grows downward from the seed [3].

Many studies have been conducted on the Ky and Cz sapphire growth methods. Timofeev et al. [4,5] conducted a study on 3D simulations of the sapphire growth method and the effect of heating conditions on melt convection in a Ky furnace. Chen [6] and Demina [3] researched the effects of temperature conditions on ingot shape during growth in the Ky method. Nouri [7] investigated the interaction between the heat zone and the internal melt in the seeding process of the Ky method. These researchers focused on analyzing the growth shape of single crystal sapphire by numerical analysis, paying attention to heater arrangement and power.

The following studies are also related to growth process monitoring. Kozik and Nezhevenko [8] investigated methods for measuring the diameter of ingots during the single crystal growth of sapphire using vision system. Xiang et al. [9] proposed measuring the melt level in Cz crystal pullers using an image-based laser-triangulation measurement system. In addition, Winkler [10,11] investigated the automation of the growth furnace in the Cz method, but this research deals with partial automation after the seeding process.

As in previous papers, it is difficult to find an entirely automated process for single crystal growth. This is because the optimization of the process conditions for seeding has not been established. Most studies that used Ky and Cz methods stated that seeding was performed when the temperature field of the melt material in the growth furnace was stabilized [12–14]. Until now, the seeding process in ingot growth, which has great influence on the quality of single crystal sapphire, has depended on the experience and technique of skilled workers. The seeding process lays the foundation for ingot growth in both Ky and Cz methods, and when any defect occurs in this process, it is likely to spread to the entire ingot. So, the growth process must be standardized and stabilized to grow a single crystal sapphire of good quality.

The aim of this research was to establish and optimize the conditions of the seeding process in the Ky method. The vision system and algorithm were developed to detect the exact time when the internal convection of the melt is stabilized by observing the shape of the spoke pattern on the melt surface. The possibility of sapphire process automation was also examined and applied to the growth furnace.

2. Principles

2.1. Detection of Auto Seeding Point in Ingot Growth

In single crystal sapphire growth methods that use a cylindrical crucible, such as Ky and Cz, a stream line generated from the edge to the center of the crucible on the surface of the melt when convection occurs (after the internal alumina is fully molten). This melt material flows because of the temperature gradient caused by the heater of the outer crucible. Generally, the flow rises on the surface of the crucible wall and moves to the center of the crucible before descending. As convection progresses, multiple stream lines enter through the center of the crucible, forming a spoke pattern [4,15]. The center of the spoke pattern where the melt flow descends is called the island. This pattern on the surface of the melt is also measured in sapphire growth methods that apply heat to a cylindrical crucible in axial symmetry [16–18]. Furthermore, this spoke pattern is measured in natural convection phenomena [19].

If the temperature field of the melt in the growth furnace is stabilized, then convection in the growth furnace is stabilized, and the island is located in the center of the crucible during growth as shown in Figure 1. The seeding process in the Ky method succeeds only when the top-down melting movement is dominant at the seeding point on the melt surface. Upward melt flow at the seeding point cause the seed to melt [20]. Therefore, if the position of the island on the surface of the melt can be measured automatically, the time when the internal convection of the melt is stabilized and when the seeding process is initiated can be detected

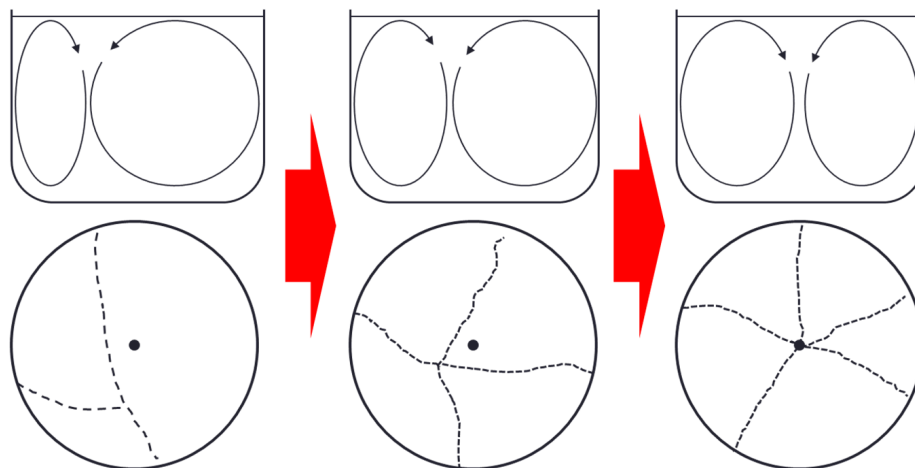


Figure 1. Spoke patterns on the surface of the melt according to temperature distribution in the crucible.

2.2. Image Processing Algorithm

The sapphire growth process of the Ky method consists of the following stages: the heating stage, in which alumina is put into the crucible and heated; the melting stage, in which the alumina is molten; the seed preparation stage, in which the temperatures of melted alumina, stream lines, and island position are observed to prepare for seeding; and the seed descending stage. Seed cleaning occurs through the first contact between the seed and the melt, and the second contact between the seed and the melt for sapphire growth.

The process observed in this study is the seed preparation stage. In this process, the worker generally monitors the surface of the melt in the growth furnace through a view point with the naked eye. Convection becomes activated from the heater around the crucible after the internal alumina is fully molten. At this time, stream lines begin to form in areas where the temperature is lower than the surrounding areas on the surface of the melt, and a spoke pattern can be observed as a result. When the melt material temperature inside the growth furnace is stabilized, the convection of the alumina melt is also stabilized, and the island, is located at the center of the growth furnace crucible. Then, when the island size grows to 10–20 mm, seeding begins. To detect the seeding point accurately, a technique is required for automatic detection of island size and the time when the center of the island coincides with the center of the crucible.

To measure the melt surface inside the growth furnace using an image, a charge coupled device (CCD) camera is installed at a view point on the top of the growth furnace. However, due to the location and size of the view point, only a portion of the actual melt material surface can be measured as shown in Figure 2.

Therefore, an algorithm was developed to measure the shape of the spoke pattern from a limited field of vision, to detect stream lines using various data obtained from the surface of the melt, and to measure the island, or the intersection point of the stream lines

The image processing procedure is divided into the image preprocessing stage, in which the collected images are binarized, and the image processing stage in which the center point of the island is traced through binarized data, as shown in Figure 3.

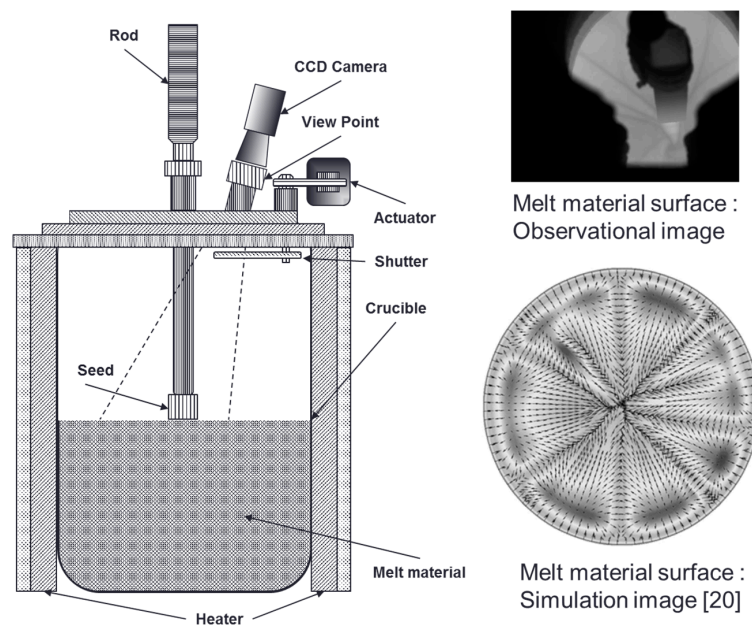


Figure 2. Comparison of the spoke pattern and observed pattern on the surface of the melt.

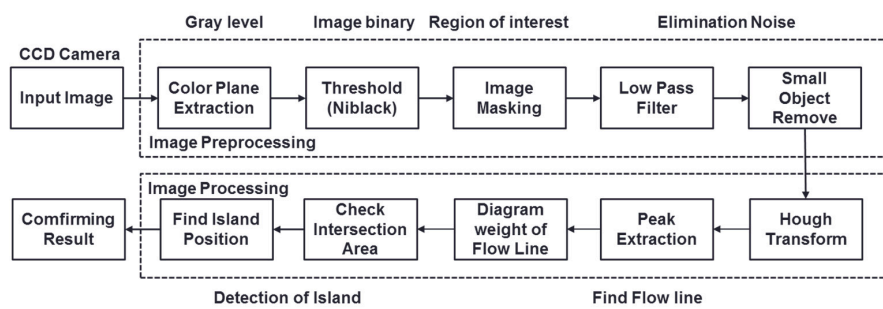


Figure 3. Image processing procedure to find the center point of the spoke pattern.

Image preprocessing is not only important for acquiring accurate stream-line data, but is also related to the accuracy of the measured data. The luminance plane is extracted to obtain information related to the brightness of the melt surface, which is obtained from the CCD camera images. The extracted image goes through a binarization process that distinguishes particles (stream lines) from non-particles (background). Global binarization, which is one of the image binarization methods that uses threshold values, provides the advantage of minimal computation. However, both the surface temperature distribution and brightness of the extracted image are irregular. It is difficult to obtain accurate stream-line data through global binarization alone. Hence, the Niblack binarization algorithm is used to overcome this condition. Niblack binarization takes threshold values by region and then performs binarization. The Niblack binarization equation is shown below:

$$(x, y) = m(x, y) + k \cdot s(x, y) \tag{1}$$

In this equation, $m(x, y)$ and $s(x, y)$ denote the average and standard deviation in a regional window, and k denotes the user defined variable for binarization. Niblack binarization determines the critical value using the average and standard deviation of pixel values inside the regional window, and the parts above the threshold value are extracted by comparing the critical value with the original image; these parts are then binarized.

In this study, the deviation value of 0.2 was used in a window with 32×32 pixels. Because the parts detected on the image are stream lines with low temperatures, dark objects were extracted.

After binarization, a mask method is used to delete data associated with the rod part, in which the seed is mounted, and the outer parts, which are not necessary for the measurement of stream lines on the surface of the melt. The region of interest is extracted from the original image using the mask method after binarization because the boundary line in the image may appear as data if binarization is performed after extraction.

After the region of interest is extracted, noise elements, excluding the stream lines on the melt surface, are removed using a low-pass filter and pixel size. Figure 4 shows the image preprocessing process.

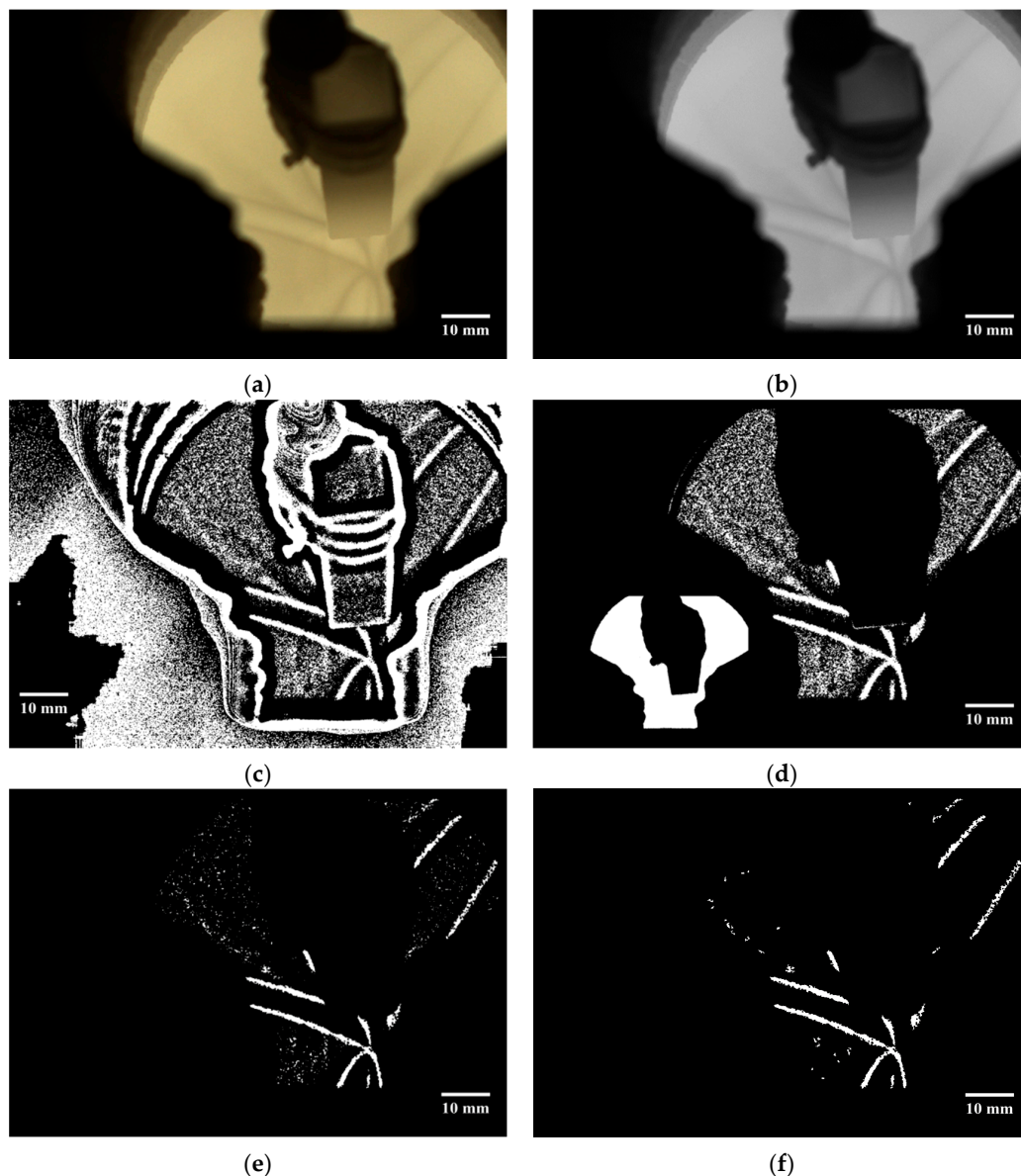


Figure 4. Image preprocessing procedure: (a) acquiring image information; (b) extracting brightness information; (c) the binarization process; (d) extracting the region of interest; (e) removal of noise elements; (f) result of image preprocessing.

The stream lines on the surface of the melt are distinguished through image preprocessing procedures. In the next image processing stage, the island position is traced using stream lines.

First, through the Hough transform of the acquired pixel data, a straight line representative of each stream line is extracted. The Hough transform is illustrated in Figure 5. One point on the x - y coordinate system appears as one curve on the ρ - θ coordinate system, and one straight line on the x - y coordinate system is expressed as one point on the ρ - θ coordinate system. The region with the highest number of intersection points on the ρ - θ coordinate system is judged as a straight line in the x - y coordinate system, and a straight line in the image is detected in this way.

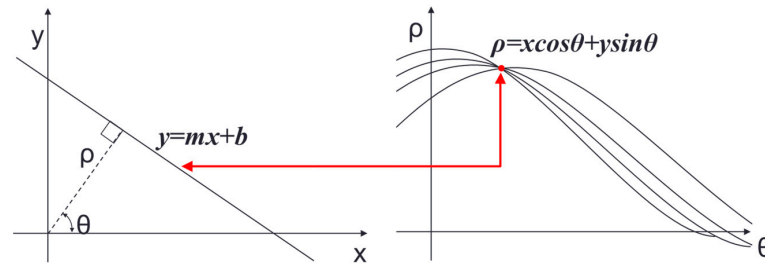


Figure 5. Principle of Hough transform.

Figure 6 shows the image processing procedure for detecting the position of stream-line intersection. Figure 6a shows an image that underwent the preprocessing procedure on the ρ - θ coordinate system. Figure 6b shows a histogram that represents the number of intersections of each curve. The region with a large number of intersections of curves on the ρ - θ coordinate system is actually expressed as a straight line on the x - y coordinate system. Thus, representative peak values are selected from each intersection region and moved to the x - y coordinate system region to generate straight lines as shown in Figure 6c. In particular, because too many straight lines are likely to appear, only points that have 100 or more intersections are transformed into straight lines, as shown in Figure 6c. Furthermore, the intersection count of curves on the ρ - θ coordinate system is assigned to each straight line as a weight value.

Figure 6d shows the stage in which the coordinates of the island center are detected using the straight line data from the x - y coordinate system acquired in the previous stage. To scan the entire image, a circular region of 20×20 pixels is created on the x - y coordinate. At this time, the intersections in the scanned region are detected and the sum of the weight values of the straight lines involved in the creation of each detected intersection is calculated. However, if the same straight line is included twice when summing the weights of straight lines, it is calculated only once. The region that has the largest sum of intersection weights in the inspected image is detected and the center of the intersections in that region is calculated; this is represented as the coordinate of the island center in the growth furnace melt material. Table 1 shows the parameter of image processing to find the center point of the spoke pattern.

Table 1. Parameter of image processing.

Image Porcessing	Parameters	Value	
	Color Plane Extraction	HSL (Luminance Plane)	
Image binarization	Local threshold (Niblack)	: Kernel size : Deviation factor	
	Low-pass filter	: Filter size : tolerance	
	Removal small objects	: Iterations	1
		: Pixel frame shape : Connectivity	Square frame (3 pixel \times 3 pixel) 4 (Horizon or vertically adjacent)
Hough transform	Threshold	100	
		20 \times 20 (Circular)	

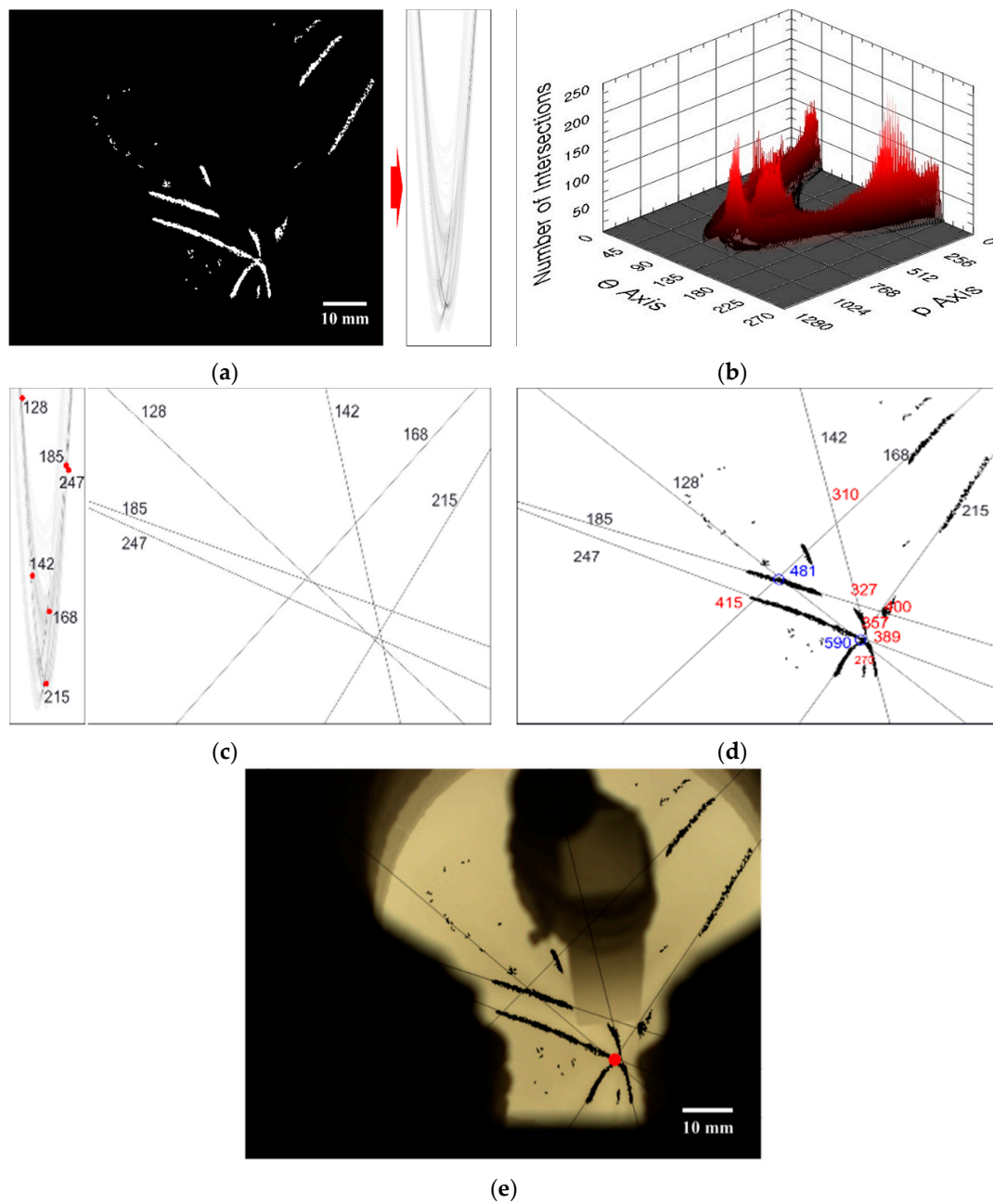


Figure 6. Image processing algorithm for detecting the island center point: (a) Hough transform; (b) intersection histogram; (c) straight line generation on x - y ; (d) detection of central point; (e) detection of island center point from the original image.

3. Experiment Method and System Composition

In the experiment, 32 kg grade sapphire growth equipment (Insight 200, ASTEK, Jeonnam, Korea) was used, and the crucible diameter is 200 mm. Figure 7 shows the single crystal growth of sapphire using the Ky method, as well as a sapphire ingot. In this study, the Ky method was used to measure the surface of the melt in the seed preparation stage of sapphire growth. The experimental system was set up as shown in Figure 8. This system consists of the following: a vision module unit, which consists of a CCD camera to take photographs of the melt material surface and a frame grabber to convert the CCD camera images into processable signals; the shutter module unit, which has a shutter

and a pneumatic actuator for damage prevention; and the motion module unit, which measures the location of the seed and moves the seed up and down for seeding.



Figure 7. The single crystal growth of sapphire using the Ky method.

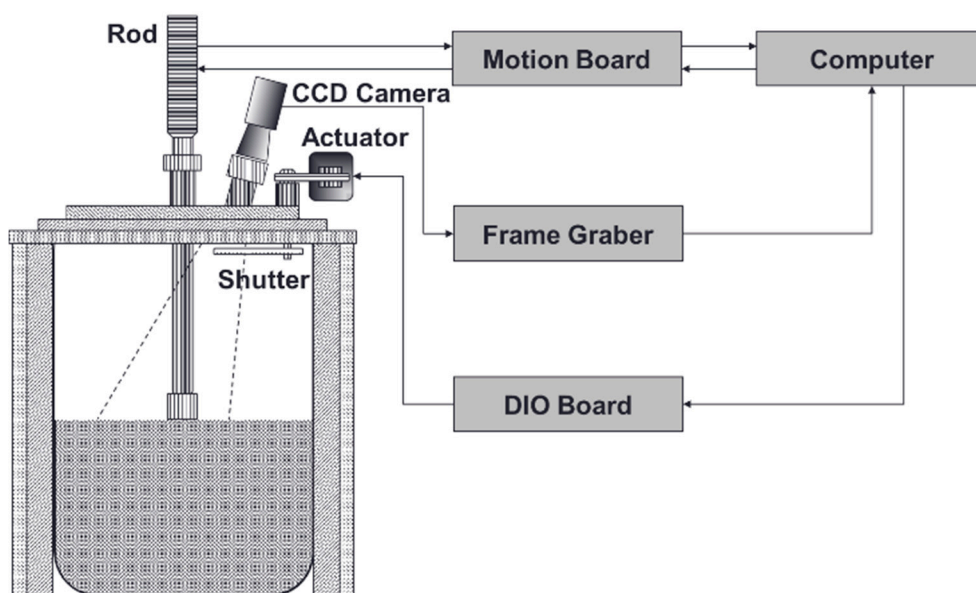


Figure 8. Block diagram of the auto seeding system.

The CCD camera used in this experiment (model UI-6230SE, IDS, Obersulm, Germany) has a resolution of 1024×768 pixels and an image capture speed of 40.0 fps. The amount of light that enters the camera was reduced using a neutral density filter (ND filter) because intense light is generated inside the growth furnace at 2000 °C or higher after alumina melting and before temperature stabilization. The collected image signals are processed through an algorithm in a controlled PC and the results are analyzed to detect the central point. Shutter open/close control signals and rod up-and-down movement commands are issued through the PC.

The experiment progressed as shown in Figure 9. The camera shutter open/close cycle is 5 s, and the total cycle takes just one minute, during which the surface images are collected and analyzed.

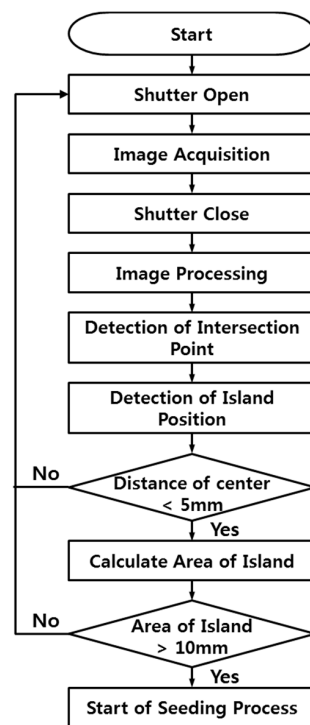


Figure 9. Flowchart of the auto-seeding process.

4. Results

During sapphire growth in the Ky method, images were acquired from the melt surface of the alumina material using the proposed system, and the coordinates of the stream-line center were processed through an image processing algorithm. After the melt material caused convection and before it was stabilized, 10 images were acquired at 5 min intervals. Figure 10 shows four representative images among the 10 images that resulted from the calculation using the algorithm. To determine the reliability of the image processing results, the island positions (shown by a green triangle) were compared with the central point positions of stream lines detected through the developed algorithm (shown by a red circle) in the figures.

The black regions obtained from image preprocessing represent the data of stream-line areas, which had low temperatures in the original image. Noise elements are generated in certain regions (see Figure 11) from the stream-line, depicted as black dots. This is one problem associated with image binarization. These noise elements are generated from the results of binarization using regional threshold values. Most noise can be removed by a low-pass filter and by removing pixels under a certain pixel value. However, large black regions are not removed, as shown in the Figure 11. When these noise elements are calculated together with other stream-line elements in the Hough transform, unintended straight lines may be generated, causing a problem in the calculation of intersection points. Yet such unremoved shades are not a serious concern when detecting the center point of the island because their intersection count is smaller than that of the actual stream-line elements. Also, they do not appear as main straight lines on the ρ - θ coordinate system.

When the observed and detected islands were compared, in most cases, the coordinates of two points were on the main stream lines, but coordinate errors occurred according to the shape of the stream-line intersection positions. When stream lines intersected in the shape of a straight line, there was about a 7-pixel (approximately 0.7 mm) error for the island coordinates. However, when the stream lines intersected in a vortex shape, as shown in Figure 12, a maximum error of 13.93 pixels (approximately 1.4 mm) occurred in the distance between the actually observed coordinates and the coordinates obtained from the algorithm.

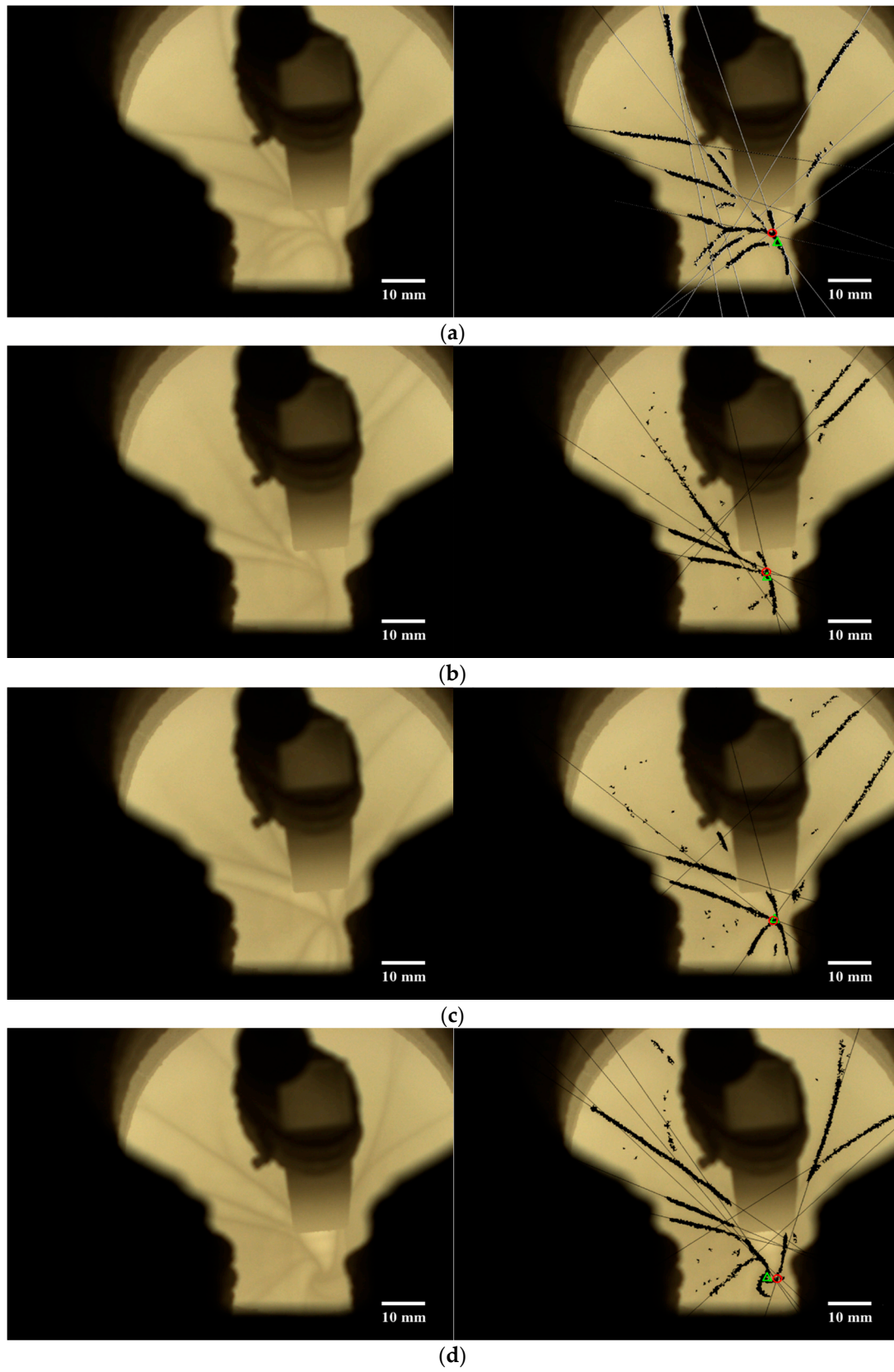


Figure 10. Image processing results of the melt surface. (Red: island position, Green: position of image processing result).

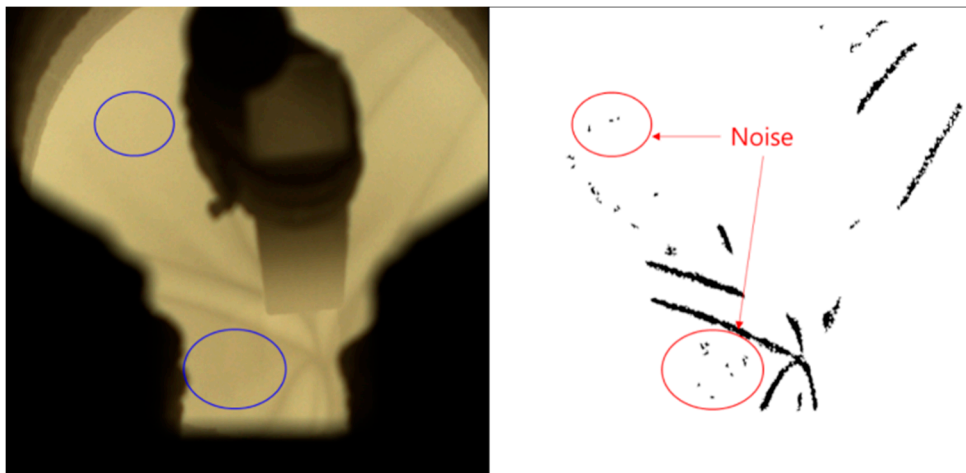


Figure 11. Noise elements after image preprocessing.

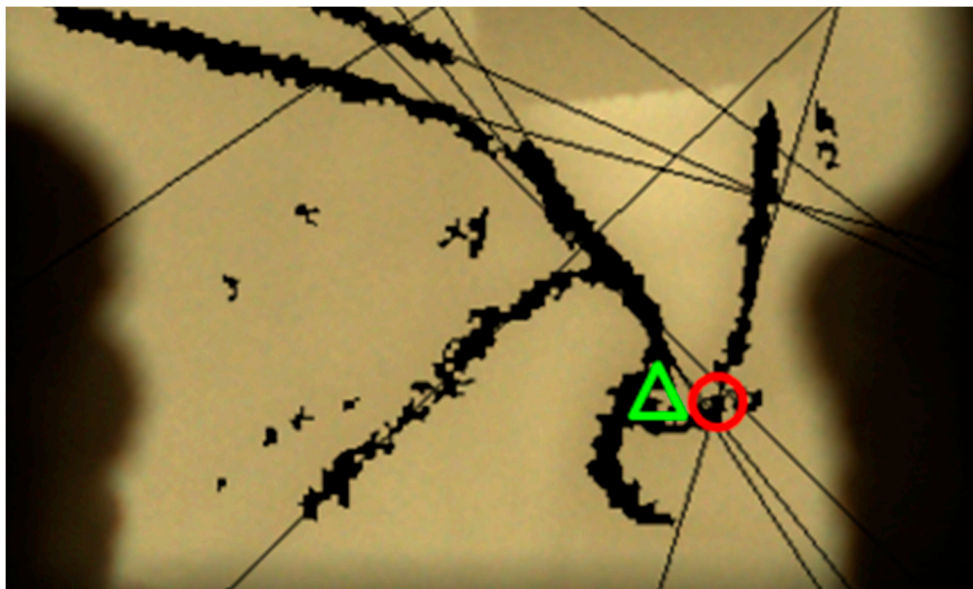


Figure 12. Error detection at the curved parts of stream lines. (Red: island position, green: position of image processing result).

Ten images were acquired from the time the surface began to melt inside the growth furnace. The positions for the center point of the island as observed and as detected through the image processing algorithm are shown in Figure 13. Table 2 shows the coordinates of the island as observed and as detected from the algorithm, as well as the distance between the coordinates in pixels. The difference ranged from 6.32 pixels (at the minimum) to 34 pixels (maximum), and the average difference was 18.76 pixels, which is about 1.9 mm in actual distance. One explanation for these differences between the two coordinate values is because the stream-line information at the center of the image was lost: about 25% of the region visible through the view point is occupied by the shape of the rod and seed, as shown in Figure 14, resulting in lower accuracy.

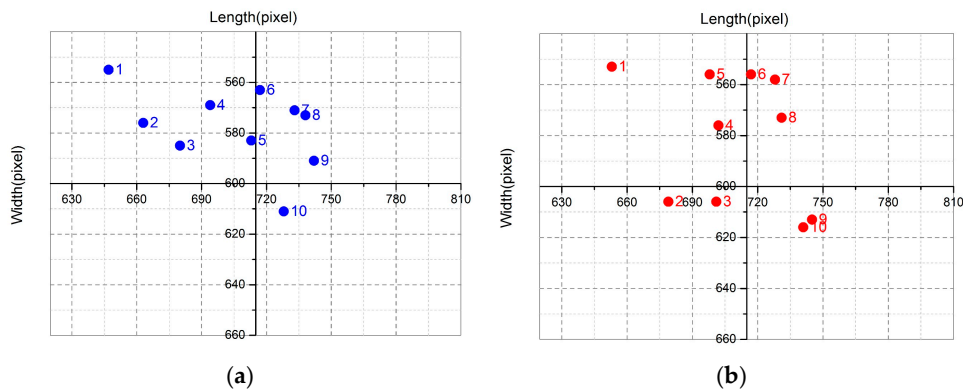


Figure 13. Changes of island positions at the center of the growth furnace crucible: (a) observed positions; (b) the positions resulting from image processing.

Table 2. Comparison of coordinates between observed and measured positions (i.e., the results of image processing).

No.	Observed Positions	Measured Positions (Image Processing Results)	Distance between the Coordinates/Positions (in Pixels)
1	(647, 555)	(653, 553)	6.32
2	(663, 576)	(679, 606)	34.00
3	(680, 585)	(701, 606)	29.70
4	(694, 569)	(702, 576)	10.63
5	(713, 583)	(698, 556)	30.89
6	(717, 563)	(717, 556)	7.00
7	(733, 571)	(728, 558)	25.94
8	(738, 573)	(731, 573)	7.00
9	(742, 591)	(745, 613)	22.20
10	(728, 611)	(741, 616)	13.93

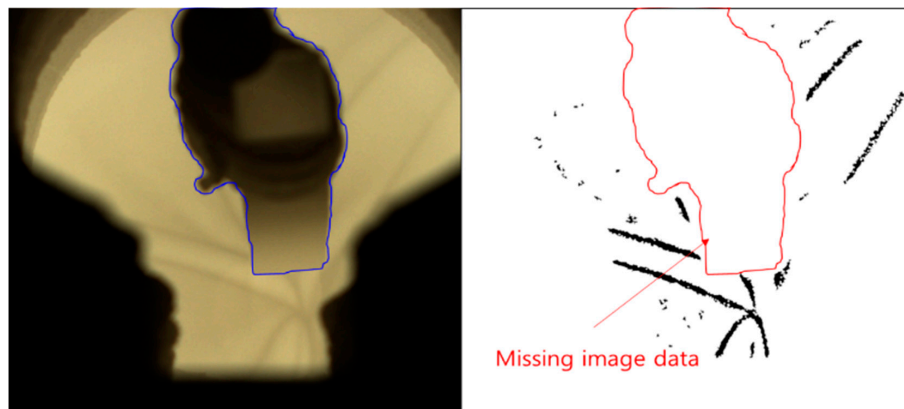


Figure 14. Loss of stream-line data caused by the outline of the rod and seed.

In general, the internal convection of the melt material was stabilized after about 20 h in the heating process, and the center position of the island in the melt material is within 10 mm of the center of the crucible in the growth furnace. After that, when the island size grows to 10–20 mm, the seed is lowered. Figure 15 displays the distance between the center of the island observed by the naked eye and the center of the island detected from the algorithm taken from images acquired during sapphire growth at the center position (750, 600) of the growth furnace crucible. All the island centers were within 10 mm of the center of the growth furnace crucible. They approached the center of the crucible over time and continuously moved at distances of 2–3 mm.

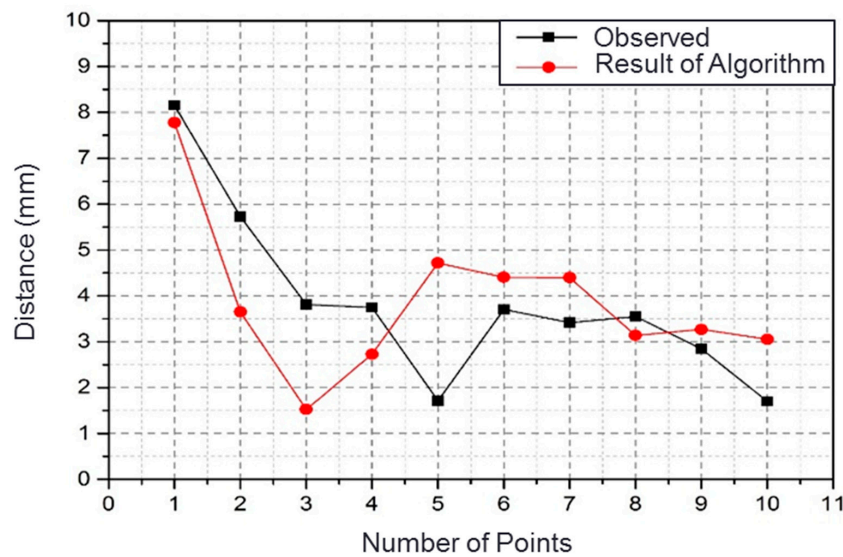


Figure 15. Distance from the center of the crucible in the growth furnace to the island center point.

5. Conclusions

In this study, an alumina melt material surface measuring system was constructed that utilized a vision system for auto seeding in a single crystal sapphire ingot growth furnace using the Ky method. Furthermore, the island position of the melt material was detected using the developed image processing algorithm, and its performance was evaluated.

To periodically acquire images of the alumina melt material surface during sapphire growth, an experimental system was constructed with a vision module unit that contained a CCD camera, a shutter module unit to protect the camera, a motion module unit for the seeding process, and the PC control unit for total system control. The images were stably acquired through this system.

The stream lines and background regions on the alumina melt material surface were detected separately using an image-processing algorithm, and the island center coordinates were calculated using the intersections of the stream lines.

When the observed coordinates of the island center were compared with the coordinates detected from the image processing algorithm, there was an average error rate of 1.87 mm (based on 1024×768 pixels). The reason for this was that the accuracy level dropped for observed coordinates compared to algorithmically detected coordinates when some stream lines intersected in a vortex shape and when the detection of stream lines was limited due to the outline of rod and seed shapes in the visual field. However, since the maximum error was about 3 mm when converted to actual distance, this error did not cause a significant problem in judging the stable condition of the internal convection of the melt material during the actual growth furnace process.

Considering the above results, the vision system and algorithm could be applied to the heater type growth method of axial symmetry in a circular cylindrical crucible using the Cz method as well as the Ky method. When applied to an actual system, these results can provide objective indicators for the seeding preparation process during sapphire growth. If the problems discovered in this study are addressed, such as the limited field of view and the error occurring in the curved parts of stream lines, automated techniques for the seeding process as well as the entire process of single crystal sapphire growth will be possible.

Author Contributions: C.M.K. and S.R.K. conceived and designed the experiments; C.M.K. performed the experiments; C.M.K., S.R.K. and J.H.A. analyzed the data; C.M.K. wrote the paper.

Conflicts of Interest: The authors declare no conflict of interest.

References

1. Tang, H.; Li, H.; Xu, J. *Growth and Development of Sapphire Crystal for LED Applications*; InTech: Rijeka, Croatia, 2013.
2. Golubovic, A.; Nikolic, S.; Djuric, S.; Valcic, A. The growth of sapphire single crystals. *J. Serbian Chem. Soc.* **2001**, *66*, 411–418.
3. Demina, S.E.; Bystrova, E.N.; Lukanina, M.A.; Mamedov, V.M.; Yuferev, V.S.; Eskov, E.V.; Nikolenko, M.V.; Postolov, V.S.; Kalaev, V.V. Numerical analysis of sapphire crystal growth by the Kyropoulos technique. *Opt. Mater.* **2007**, *30*, 62–65. [[CrossRef](#)]
4. Timofeev, V.V.; Kalaev, V.V.; Ivanov, V.G. 3D melt convection in sapphire crystal growth Evaluation of physical properties. *Int. J. Heat Mass Transf.* **2015**, *87*, 42–48. [[CrossRef](#)]
5. Timofeev, V.V.; Kalaev, V.V.; Ivanov, V.G. Effect of heating conditions on flow patterns during the seeding stage of Kyropoulos sapphire crystal growth. *J. Cryst. Growth* **2016**, *445*, 47–52. [[CrossRef](#)]
6. Chen, C.H.; Chen, J.C.; Lu, C.W.; Liu, C.M. Effect of power arrangement on the crystal shape during the Kyropoulos sapphire crystal growth process. *J. Cryst. Growth* **2012**, *352*, 9–15. [[CrossRef](#)]
7. Nouri, A.; Delannoy, Y.; Chichignoud, G.; Lhomond, L.; Helifa, B.; Lefkeir, I.K.; Zaidat, K. Numerical investigation of an experimental Kyropoulos process to grow silicon ingots for photovoltaic application. *J. Cryst. Growth* **2017**, *460*, 48–58. [[CrossRef](#)]
8. Kozik, V.I.; Nezhevenko, E.S. Measuring silicon monocrystal diameters during melt growth. *Optoelectron. Instrum. Data Process.* **2008**, *44*, 392–401. [[CrossRef](#)]
9. Xiang, S.; Pan, F.; Xiang, K.; Wang, X. Melt level measurement for the CZ crystal using an improved laser triangulation system. *J. Meas.* **2017**, *103*, 27–35. [[CrossRef](#)]
10. Winkler, J.; Robenack, K. Observer based determination of the crystal diameter in Czochralski crystal growth utilizing algorithmic differentiation. In Proceedings of the Systems, Signals and Devices (SSD), 2012 9th International Multi-Conference, Chemnitz, Germany, 20–23 March 2012; pp. 1–6.
11. Winkler, J.; Neubert, M.; Rudolph, J. A review of the automation of the Czochralski crystal growth process. *Acta Phys. Pol.* **2013**, *124*, 181–192. [[CrossRef](#)]
12. Xu, C.H.; Zhang, M.F.; Meng, S.H.; Han, J.C.; Wang, G.G.; Zuo, H.B. Temperature field design, process analysis and control of SAPMAC method for the growth of large size sapphire crystals. *Cryst. Res. Technol.* **2007**, *42*, 751–757. [[CrossRef](#)]
13. Wang, G.; Zuo, H.; Zhang, H.; Wu, Q.; Zhang, M.; He, X.; Hu, Z.; Zhu, L. Preparation, quality characterization, service performance evaluation and its modification of sapphire crystal for optical window and dome application. *Mater. Des.* **2010**, *31*, 706–711. [[CrossRef](#)]
14. Chenghai, X.; Songhe, M.; Mingfu, Z.; Hongbo, Z.; Guigen, W. Thermal Stresses and Cracks During the Growth of Large-sized Sapphire with SAPMAC Method. *Chin. J. Aeronaut.* **2007**, *20*, 475–480. [[CrossRef](#)]
15. Demina, S.E.; Kalaev, V.V. 3D unsteady computer modeling of industrial scale Ky and Cz sapphire crystal growth. *J. Cryst. Growth* **2011**, *320*, 23–27. [[CrossRef](#)]
16. Jing, C.J.; Imaishi, N.; Yasuhiro, S.; Miyazawa, Y. Three-dimensional numerical simulation of oxide melt flow in Czochralski configuration. *J. Cryst. Growth* **2016**, *216*, 372–388. [[CrossRef](#)]
17. Jing, C.J.; Imaishi, N.; Yasuhiro, S.; Miyazawa, Y. Three-dimensional numerical simulation of spoke pattern in oxide melt. *J. Cryst. Growth* **1999**, *200*, 204–212. [[CrossRef](#)]
18. Kobayashi, M.; Tsukada, T.; Hozawa, M. Effect of internal radiative heat transfer on the convection in Cz oxide melt. *J. Cryst. Growth* **1997**, *180*, 157–166. [[CrossRef](#)]
19. Miller, D.C.; Pernell, T.L. Fluid flow patterns in a simulated garnet melt. *J. Cryst. Growth* **1982**, *58*, 253–260. [[CrossRef](#)]
20. Numerical Analysis and Optimization of Sapphire Crystal Growth by the Kyropoulos Technique. Available online: http://str-soft.com/products/CGSim/Kyropoulos_Sapphire/index.htm (accessed on 16 March 2017).

